Journal of Petroleum Science and Engineering 108 (2013) 267–278

Contents lists available at ScienceDirect

Journal of Petroleum Science and Engineering

journal homepage: www.elsevier.com/locate/petrol

Permeability from porosimetry measurements: Derivation for a tortuous and fractal tubular bundle

J.J.M. Buiting *, E.A. Clerke

Geological Modeling Division, Reservoir Characterization Department, Saudi Aramco, P.O. Box 11391, Dhahran 31311, Saudi Arabia

ARTICLE INFO

Article history:
Received 20 November 2011
Accepted 26 April 2013
Available online 14 May 2013

Keywords:
carbonate
permeability
pore-throat sizes
tortuosity
fractal
capillary pressure

ABSTRACT

Permeability modeling of complex carbonate reservoirs is difficult. Porosity–permeability relationships are weak in carbonates and conventional porosity–permeability transforms give poor results. Even though the link between porosity and permeability in carbonates persists, other pore system properties, such as the largest connected pore-throat diameter, are more strongly linked to permeability. This important pore-throat diameter, as well as related porosity and other pore system architectural information, is determined by the analysis of mercury injection capillary pressure (MICP) porosimetry experiments. This paper explores the use of porosimetry data for the calculation of permeability as originally demonstrated by Purcell in 1949. We return to the tubular bundle model of Purcell and Burdine with a general mathematical form for the porosimetry data and a new tortuous and fractal relative tubular bundle. Using mathematical reasoning, without fitting parameters, we obtain a new formula for the computation of permeability based on the pore system architectural information of highly connected systems using the MICP porosimetry data. Moreover, we include the observation that the flow paths and the related tortuosity have a fractal aspect. The result is compared to an extensive porosimetry data set of the highly connected Arab D limestone, where vugs are absent. For porous media characterized by porosimetry data, the following expression emerges:

$$\kappa \approx 506 \frac{B_v^{\infty}}{P_d^2} e^{-4.43\sqrt{G}},$$

which is the permeability for a monomodal carbonate pore system characterized by a single Thomeer hyperbola with associated Thomeer parameters (κ is in Darcy; B_v^{∞} in fractional bulk volume, and P_d is the minimum entry pressure in psi and G is the pore-geometrical factor). The nearly equal sign is used here only because of an approximation used for the modified Bessel function of the second kind present in the general solution and approximate knowledge of the fractal exponent and the percolation path length ratio. There are no fitting factors. The exponents on the variables in our permeability formula demonstrate the significant shift in emphasis from porosity to the diameter of the largest connected pore throats, P_d. Note that the presence of vugs are not considered in this work, since they do not form part of the Arab-D limestone matrix.

This mathematical effort emphasizes the relative importance of pore system attributes on permeability as commonly found in carbonate porosimetry data. The approach can be readily extended to multimodal carbonate pore systems, to other sources of pore system architectural data and is shown to be equivalent to the operation of an incomplete Laplace transform on the porosimetry data. Importantly, and in contrast to previous permeability models to which we compare, this new formulation sets the stage for a complete and scale independent understanding of permeability in carbonate pore systems commonly encountered in the Arab D limestone and similar pore systems.

1. Introduction

The carbonate oil reservoirs of Saudi Arabia are the most prolific in the world. Their porosities and permeabilities are excellent, but detailed understanding of the petrophysical properties of these complex carbonate pore systems is insufficient. The carbonate pore systems are complex and multimodal (Cantrell and Hagerty, 1999; Cantrell and Hagerty, 2003; Clerke et al., 2008) leading to poor porosity–permeability relationships. Standard porosity–permeability transforms have major and well-known shortcomings (Delfiner, 2007) especially in the case of carbonates. Estimating accurate matrix permeability for the Arab-D limestone

* Corresponding author. Tel.: +966 500378390, +966 3 8737950.
E-mail addresses: johannes.buiting@aramco.com (J.J.M. Buiting), edward.clerke@aramco.com (E.A. Clerke).

0920-4105/$ - see front matter © 2013 Elsevier B.V. All rights reserved.
http://dx.doi.org/10.1016/j.petrol.2013.04.016

from porosity alone is unsatisfactory (Clerke et al., 2008; Clerke, 2009). Additional information about the pore systems is needed. Saudi Aramco has acquired many mercury injection capillary pressure (MICP) porosimetry data on Arab D limestone core plugs (Clerke et al., 2008), which are analyzed using the method proposed by Thomeer (1960) who observed a hyperbolic relationship between the fractional bulk volume of injected mercury, log (B_v) and the applied mercury pressure, log(P_c). The amount of mercury entering a single pore system in an MICP experiment, expressed as the fractional bulk volume occupied B_v, exhibits a distinct hyperbolic shape. Thomeer's observation is represented by his empirical formula:

$$B_v(P_c)\approx B_v^{\infty}\exp\left(\frac{-G}{\log(P_c)-\log(P_d)}\right) \quad \text{for } P_c > P_d;\ 0 \text{ elsewhere.} \tag{1}$$

The details in position and shape of the hyperbola are determined by the three Thomeer parameters: P_d, which is the "minimum entry pressure" or "threshold pressure", related to the largest connected pore throat diameter; G is the "pore geometrical factor" related to the range of pore throat diameters and B_v^{∞}, which is the "fractional bulk volume occupied" by mercury at $P_c=\infty$. P_c is the applied mercury pressure, normally in psi.

These three pore system parameters determine the pore geometrical capillary forces within the reservoir pore system and exert important control on the original distribution of water and oil within the reservoir pore system. This significant pore geometrical information must also contain the information regarding the flow of liquids through the reservoir and thus largely define absolute permeability. This realization was introduced by Purcell (1949) and Burdine (1953) and later successfully developed by Thomeer (1983) and Swanson (1981), and others (Huet et al., 2005), despite the fact that pseudo-static MICP data do not give explicit information on the accessibility, complexity and tortuosity of the flow paths. Our efforts expand upon that of previous workers by using rigorous mathematics and by introducing a tortuous and fractal relative tubular bundle. The result is a completely new functional form for permeability. We proceed to compare our new formulation to abundant Arab D carbonate MICP data (Clerke et al., 2008).

2. Permeability of a tortuous tubular bundle

We represent the actual pore system by an assortment of different tubes, connecting one end of the rock to the other, starting with the approach of Purcell (1949), Burdine (1953), and Calhoun et al. (1949). In Appendix A, a step-by-step derivation is given. It leads ultimately to the general equation, which will be summarized in this section.

The total volume of liquid passing through a piece of rock of length, L, and cross-sectional area, A, is described by the standard Muscat–Darcy fluid-flow equation as

$$\frac{dV_{liq}}{dt}=\frac{\kappa A}{\mu L}\Delta P, \tag{2}$$

where μ is the viscosity of the liquid and ΔP is the pressure drop over the length of the tube. κ is the permeability which needs to be expressed in terms of fundamental rock properties, such as porosity and pore architectural parameters.

Under a pressure gradient, liquids flow through a porous rock along certain paths, which are envisaged as well-defined pipes or tubes. We assume that the flow is non-turbulent. In this tubular bundle representation of a rock pore system, the tubes connect one side of the rock sample with the other. It is assumed that the tubes have varying dimensions, different radii, r_i, and different lengths L_i. Moreover, the tubes are tortuous and not straight, so that the length of a tube is longer than the sample outer length, i.e. $L_i > L$.

The tubes are identified by their radii, r_i. Within the "i-family", there are n_i tubes. Each tube of radius r_i can in principle have a different length. However, here, we assume that they all have the same length L_i, where L_i is an average length of all the tubes with radius r_i.

The lengths of the tubes are also modeled to increase with decreasing diameters, i.e. $L_{i+1} > L_i$ (throughout this paper we use the convention that the radius decreases with increasing index i, i.e. $r_{i+1} < r_i$). This is reasonable because the flow paths through the narrower passages of the pore system are expected to be more tortuous and thus longer. Moreover these tubes of narrow diameters should be more numerous, i.e. $n_{i+1} > n_i$.

The Hagen–Poiseuille flow equation for this bundle of tubes can be written as (for details see Appendix A):

$$\frac{dV_{liq}}{dt}=\sum_i n_i\frac{\pi r_i^4}{8\mu L_i}\Delta P. \tag{3}$$

From Eqs. (2) and (3), the permeability is extracted as

$$\kappa=\frac{1}{8}\sum_i n_i\frac{\pi r_i^4}{A}\frac{L}{L_i}. \tag{4}$$

The volume of a single tube with radius r_i is $v_i=\pi r_i^2 L_i$ and the volume of all the tubes with radius r_i is $V_i = n_i v_i = n_i\pi r_i^2 L_i$. The volume of the bulk rock $V_b=AL$. With these, we can rewrite (4) as

$$\kappa=\frac{1}{8}\sum_i\underbrace{\frac{n_i\pi r_i^2 L_i}{AL}}_{\Delta\varphi_i}\left(\frac{L}{L_i}\right)^2 r_i^2=\frac{1}{8}\sum_i\Delta\varphi_i r_i^2\left(\frac{L}{L_i}\right)^2, \tag{5}$$

where the incremental porosity is introduced, $\Delta\varphi_i = V_i/V_b$, which is related to all the tubes with radius r_i.

The total porosity is the sum of all incremental porosities: $\phi=\sum_i\Delta\varphi_i$, and porosity normalization yields

$$\kappa=\frac{1}{8}\phi\sum_i\frac{\Delta\varphi_i}{\phi}r_i^2\left(\frac{L}{L_i}\right)^2. \tag{6}$$

Now, we denote the properties of the largest diameter tube with the special subscript, "d". So the largest diameter tube has a radius of r_d and a length of L_d. The subscript "d" anticipates the relationship with P_d, the minimum entry pressure for mercury (threshold pressure) where in an MICP experiment the mercury first enters the largest pore throat by penetrating into the throat (s) of radius r_d.

It is now convenient to denote the dimensions of all other tubes, i.e. radii and lengths, relative to that of the largest tube in the system, by rewriting the previous equation as (see Eq. (A4))

$$\kappa=\frac{1}{8}\phi\sum_i\frac{\Delta\varphi_i}{\phi}r_i^2\left(\frac{L}{L_i}\right)^2\left(\frac{r_d}{r_d}\right)^2\left(\frac{L_d}{L_d}\right)^2\Leftrightarrow\kappa=\frac{1}{8}r_d^2\phi\left(\frac{L}{L_d}\right)^2\sum_i\frac{\Delta\varphi_i}{\phi}\left(\frac{r_i}{r_d}\right)^2\left(\frac{L_d}{L_i}\right)^2 \tag{7}$$

The contributions of the tube radii and lengths are now all referenced to the radius and length of the biggest tube in the system. It is reasonable to assume that the biggest tube has also the shortest length L_d, which is smaller than L_i. Of course L_d is larger than the length L of the sample, so that

$$0\le\frac{L_d}{L_i}\le 1 \quad \text{and} \quad 0\le\frac{r_i}{r_d}\le 1$$

Let χ_L be the relative tube parameter product defined as

$$\chi_L^2\equiv\left(\frac{r_i}{r_d}\right)^2\left(\frac{L_d}{L_i}\right)^2<1. \tag{8}$$

Then since $\sum_i\Delta\varphi_i/\phi=1$, the porosity weighted square relative tube parameter is $\sum_i\Delta\varphi_i/\phi\chi_L^2=\langle\chi_L^2\rangle$ and Eq. (7) can now be written

more compactly as

$$\kappa = \frac{1}{8} r_d^2 \phi \left(\frac{L}{L_d}\right)^2 \langle \chi_L^2 \rangle \tag{9}$$

Here it is interesting to make a comparison to the generalized Carman–Kozeny permeability (Wyllie and Gardner, 1958), which explicitly includes tortuosity. The Carman–Kozeny permeability formula is given in Eq. (10):

$$\kappa_{ck} = \frac{1}{8} r_e^2 \frac{\phi}{\tau_{ck}}, \tag{10}$$

where τ_{ck} is the tortuosity factor.

The tortuosity factor can be identified through comparison to Eq. (9) as

$$\frac{1}{\tau_{ck}} \equiv \left(\frac{L}{L_d}\right)^2 \sum_i \frac{\Delta\varphi_i}{\phi} \left(\frac{r_i}{r_d}\right)^2 \left(\frac{L_d}{L_i}\right)^2 = \left(\frac{L}{L_d}\right)^2 \langle \chi_L^2 \rangle. \tag{11}$$

It is worth mentioning that the radii r_i and r_d are related to the pressure and the first entry pressure of mercury in an MICP experiment. Also, the differential porosity $\Delta\varphi_i$, is identical to the incremental fractional bulk volume of injected mercury $\Delta B_{v,i}$.

3. Fractal tortuosity and relative tube lengths

The porosity, incremental porosity and the pore throat (tube) radii can be determined from analysis of MICP porosimetry experiments. However, the lengths of the flow paths (tubes) are not directly derived from the analysis of MICP data. Alternative methods are needed to determine these quantities which contribute to the tortuosity.

Tortuosity relates the lengths of the actual flow paths between two points to the length of the direct connection (Fig. 1), i.e. tortuosity$=L_{path}/L_{direct}$. The flow paths through the pore spaces behind the specific pore throats, represented as tubes in the bundle, are very tortuous. The flowing liquid circumvents the solid material of the rock and finds many paths to go from beginning to end (Fig. 1).

The topology of these flow paths is similar to that of other natural highly connected systems which can be directly investigated: rivers, torrents, coast lines, blood vessels, etc. These topologies are scale invariant (at least partially) and can be described using the fractal concept (Mandelbrot, 1975). Others have observed that the internal structure of porous rocks, and carbonates in particular, are fractal (Angulo et al., 1992). The lengths of fractal entities, such as river systems, blood vessel or the tortuous flow paths in a porous carbonate, are dependent on the size of the measuring rod. Classic examples are the lengths of the rugged coast lines of Britain (Mandelbrot, 1975) and Norway (Feder, 1988). The apparent lengths between two points on the coast line are vastly different when measured upon a satellite photograph versus being measured by walking along the shore line. In other words, the measured path length is different when using the photographic measuring scale of 100 km versus a human stride length of only 1 m. This is illustrated in Fig. 2.

For a fractal object, the number of rods of length ℓ required to cover the total length of a feature from start to finish is $N_{rods}^{\ell} \propto \ell^{-D_\lambda}$, where D_λ is the fractal dimension (Mandelbrot, 1975; Feder, 1988; Turcotte, 1992; Korvin, 1992). For linear features, $1 \le D_\lambda \le 2$. When $D_\lambda \approx 1$, the path is a smooth curve, not a fractal, e.g. a straight line or a circle. In the case of extreme tortuosity, ($D_\lambda \approx 2$) the path or curve fluctuates so drastically that its path covers the entire plane (e.g. Peano curves), something that does not happen in nature. For natural features such as coast lines, arteries and rivers, $1.2 \le D_\lambda \le 1.6$. An example is the coast of Britain which has a fractal dimension of 1.24 for rod lengths between 10 and 100 km. The more rugged coast line of Norway (Feder, 1988) has a fractal dimension of 1.52. A self-avoiding random walk path has a fractal dimension of 1.55. Since the flow paths in porous carbonate rocks are quite tortuous, it is anticipated that the fractal dimension will be between 1.5 and 1.8, similar to, for example, blood vessels and arteries (Boxt et al., 1994).

Knowing the numbers of rods of length ℓ covering a fractal curve, the measured length is calculated:

$$L(\ell) = N_{rods}^{\ell} \ell \propto \ell^{1-D_\lambda}. \tag{12}$$

A practical choice for a measuring rod is in some case quite obvious. In the case of a river, the average river width is the obvious choice (it is not useful to quote the river length separately for each river bank). A smaller measuring rod would not give the river length information with any more value. When one is interested in the flow of the water or the routes of boats, a rod length of about the width (or half the width) of the river is appropriate.

A similar argument gives the appropriate rod length for the tortuous flow paths of blood through arteries or of oil flowing through the tubular pore system of a porous rock. If such a tortuous tube system is a natural fractal, then the power law of

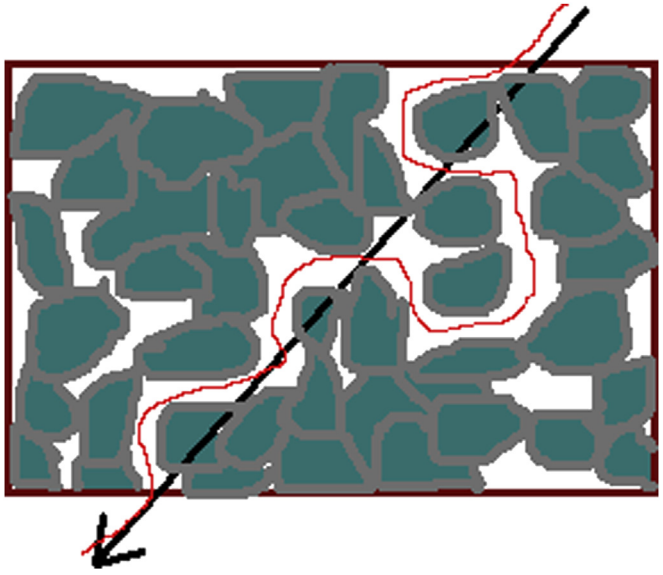

Fig. 1. Tortuous flow path through a rock (red). The black line is the direct connection. (For interpretation of the references to color in this figure legend, the reader is referred to the web version of this article.)

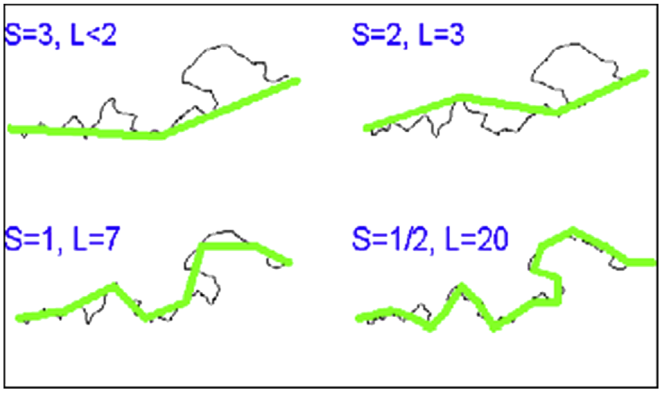

Fig. 2. Measuring the length (L) of a tortuous line with a measuring rod of different sizes (S). The measured lengths get larger with smaller rod.

Eq. (12) holds for a wide range of ℓ values. The bulk of the liquid flowing through a pore system will follow a central route through the flow path or tube. An appropriate measurement length ℓ would be the radius r of the tube, so the apparent length of a tortuous tube can be usefully expressed as

$$L(r) \propto r^{1-D_\lambda}. \tag{13}$$

and specifically for our relative tubular bundle, the length of the tube/flow path related to the pore throat radius r is

$$L(r) \approx L_d \left(\frac{r}{r_d}\right)^{1-D_\lambda} \quad \text{for } r \le r_d \tag{14}$$

where L_d is the shortest flow path associated with the biggest tube of radius r_d. L_d is also the length of the first percolation path, i.e. the path or tube where the fluid first breaks through from one end of the rock to the other. It is likely that for the largest pore-throats, i.e. the biggest tubes, the fractal assumption breaks down. Nonetheless, it is assumed that the flow paths remain fractal for all sizes of the pore throats or tubes and Eq. (14) is an acceptable approximation, maintaining a sensible boundary condition of $L(r_d)=L_d$.

Using the fractal argument and the appropriate rod length, we now have an expression which relates the diameter of the tubes to their lengths in our bundle. The general permeability equation (Eq. (9)) can now be simplified, using Eq. 14 with $r=r_i$, as

$$\kappa \approx \frac{1}{8} r_d^2 \phi \left(\frac{L}{L_d}\right)^2 \sum_i \frac{\Delta\varphi_i}{\phi} \left(\frac{r_i}{r_d}\right)^{2D_\lambda} \tag{15}$$

In the above expression, tortuosity enters via the fractal dimension D_λ and the relative length of the shortest (percolation) flow path or biggest diameter tube to the sample length, the ratio L/L_d.

The length of the percolation path in our porous media is equivalent to the shortest route from one side of the rock to the other. This length is similar to the shortest route from A to B in a city like Manhattan (see Fig. 3). The length, L_d, of the route is roughly twice as long as the length L between A and B. This result is independent of the width of streets or in terms of porous rocks, independent of porosity. The building blocks in Fig. 3 can be seen as the solid grains of a carbonate rock. The L_d/L ratio of 2 is valid for angular blocks or grains. For more rounded grains L_d/L ratio would be smaller, i.e. of the order of 1.3–1.6 (Wu et al., 2006), which is roughly the value for the tortuosity of a bed of uniform spherical particles (Bird et al., 1960). Since carbonate grain shapes contain skeletal fragments, the grains are somewhat angular, it is expected that $L_d/L \approx 2$.

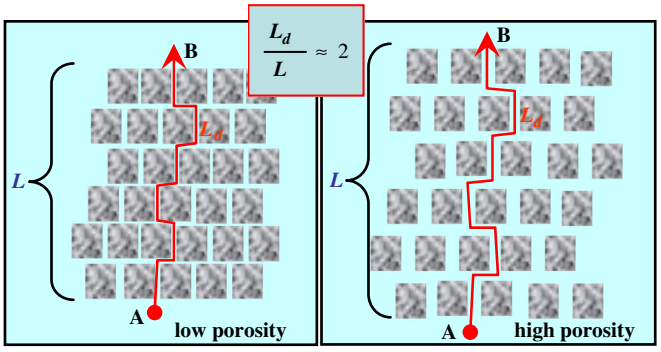

Fig. 3. The shortest (tortuous) route from A to B, while avoiding angular obstacles. This corresponds with the percolation path of a liquid passing through a porous carbonate. The tortuosity is about 2 and very weakly dependent on porosity.

4. Permeability in terms of the B_v-curve of an MICP experiment

Using Eq. (15), the tortuous and fractal relative tubular bundle model is prepared for the pore system architectural information obtained from MICP porosimetry. We now relate the radii of the tubes, r_i, to the pressure of the progressively intruding mercury, with $r \approx \xi/P$, ($\xi = 2[\sigma\cos(\theta)]_{\text{Hg–Air}} \approx 734$ dyn/cm $= 107$ psi μm) and relate the incremental porosity filled, $\Delta\varphi_i$, to the experimental $\Delta B_{v,i}$, the incremental fractional bulk volume of mercury injected at each pressure increase during the MICP intrusion experiment. The parameters required by our equation (15) are determined from the experimental MICP porosimetry B_v curve. (A detailed derivation is given in Appendix B.) The result is now the general expression for the permeability from MICP porosimetry data:

$$\kappa = \frac{\xi^2}{4} D_\lambda \, e^{-2(1-D_\lambda)Q_d} \left(\frac{L}{L_d}\right)^2 \tilde{B}_v^Q(2D_\lambda). \tag{16}$$

This is an expression given in the Q-domain, where $Q=\ln(P)$, where P is the pressure of the injected mercury. The pressure on the intruding mercury is directly related to the pore throat or smallest tube radius, r, intruded by mercury, i.e. $P \approx \xi/r$ and $Q \approx -\ln(r/\xi)$. Moreover we add, $Q_d=\ln(P_d)$, where P_d ($\approx \xi/r_d$) as a convenient form for the minimum entry pressure required to intrude into the largest pore-throat radius, r_d.

$\tilde{B}_v^Q(2D_\lambda)$ is an integral transform of the MICP fractional bulk volume B_v in the Q-domain, given by

$$\tilde{B}_v^Q(2D_\lambda) \equiv \int_{Q=Q_d}^{\infty} B_v^Q(Q)\, e^{-2D_\lambda Q} dQ, \tag{17}$$

which is an incomplete Laplace transform, since the integration starts at Q_d rather than 0.

In the case $Q_d > 0$ (i.e. $P_d > 1$ psi, $r_d < 100$ μm, as is the case for most laboratory MICP data), Eq. (17) can be written as a normal Laplace transform, since $B_v(Q<Q_d)=0$, and

$$\tilde{B}_v^Q(2D_\lambda) = \int_{Q=0}^{\infty} B_v^Q(Q)\, e^{-2D_\lambda Q} dQ \equiv \hat{B}_v^Q(2D_\lambda) \tag{18}$$

In this case the permeability is now computed using the complete Laplace transform:

$$\kappa = \frac{\xi^2}{4} D_\lambda \, e^{-2(1-D_\lambda)Q_d} \left(\frac{L}{L_d}\right)^2 \hat{B}_v^Q(2D_\lambda) \tag{19}$$

The permeability for reservoir rocks from porosimetry data can be directly obtained by applying the Q-domain Laplace transform (see also Eqs. (B(19) and B20)).

4.1. Three examples: Permeability for good reservoir–poor reservoir and a step function MICP curve

Fig. 4 shows B_v porosimetry data for two 20% porosity rocks; one is a good reservoir rock with $r_d \approx 50$ μm and $P_d \approx 2$ psi ($Q_d \approx 0.7$), while the other is a poor reservoir rock with $r_d \approx 10$ μm and $P_d \approx 10$ psi ($Q_d \approx 2.3$). The exponential function in the Laplace transform of Eq. (18), i.e. $\exp(-2D_\lambda Q)$, is also displayed. The Laplace transform exponential is independent of the rock properties. The presence of $\exp(-2D_\lambda Q)$ under the integral of Eq. (18) significantly reduces the B_v contribution to the integral and thus to the permeability for the poor rock compared to good rock.

The variation of the permeability for (even equally) porous rock samples is described by the difference in the product of the MICP cumulative intrusion curves, $B_v(Q)$, with the fixed Laplace transform exponential.

Let us examine a simple case where $B_v(P)$ is a step function, $B_v(P > P_d) = \phi$ and 0 elsewhere. In the Q-domain, $B_v(Q > Q_d) = \phi$, where $Q_d = \ln(P_d)$, as is illustrated by the blue curve in Fig. 5. Such a

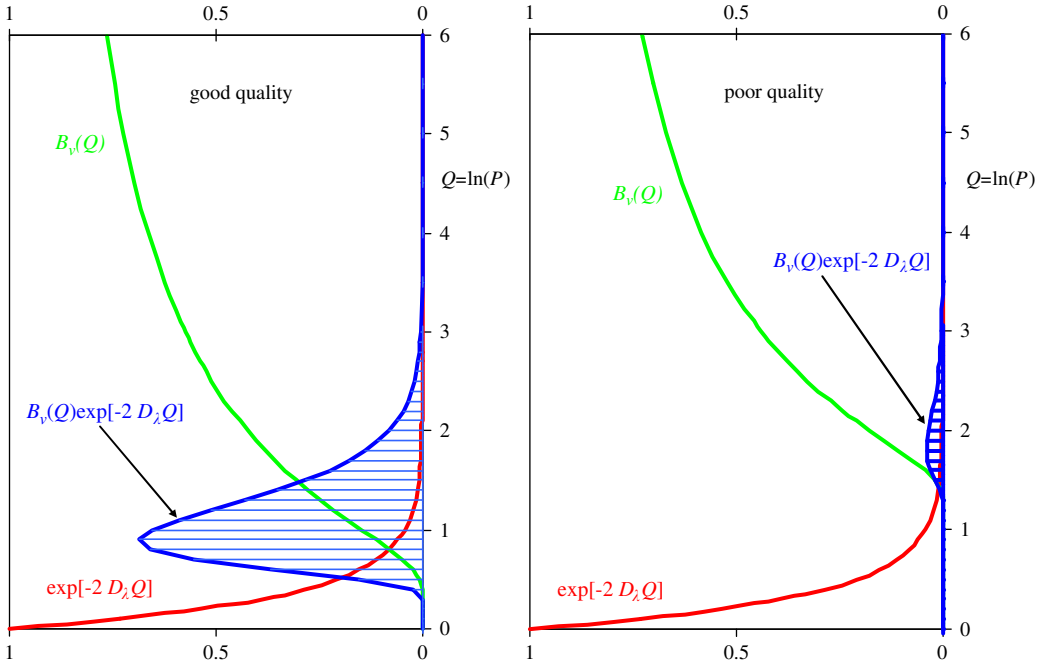

Fig. 4. The effect on the exponential of the Laplace transformation on the B_ν functions. The areas under the blue curves determining permeability. In the poorer reservoir rock the red exponential more or less annihilates the blue (permeability) curve. (For interpretation of the references to color in this figure legend, the reader is referred to the web version of this article.)

step function is in sharp contrast to a more realistic B_ν-function, shown in green in Fig. 5. The Laplace transform of the step function is

$$\hat{B}_\nu^Q(2D_\lambda) \equiv \int_{Q=0}^{\infty} B_\nu^Q(Q)\, e^{-2D_\lambda Q}\, dQ = \frac{\phi}{2D_\lambda} e^{-2D_\lambda Q_d} \tag{20}$$

So that the permeability reads (from Eq. 19), recalling that $Q_d \approx -\ln(r_d/\xi)$

$$\kappa = \frac{\xi^2}{8}\phi \left(\frac{L}{L_d}\right)^2 e^{-2Q_d} \equiv \frac{1}{8} r_d^2 \phi \left(\frac{L}{L_d}\right)^2 \tag{21}$$

This result is similar to the expression of the permeability of a single tortuous tube of length L_d and radius, r_d, in a solid.

5. Permeability in terms of the general Thomeer B_ν-curve

In the 1950s J.H.M. (Bert) Thomeer (1960) of Shell Oil observed, when analyzing MICP data from reservoir samples, that a typical hyperbolic relationship existed between the experimental log(B_ν) values and the applied mercury pressure log(P_c). The amount of mercury entering a pore system in an MICP experiment, expressed as the fractional bulk volume occupied, B_ν, exhibits a distinct shape as a function of the applied mercury pressure. These Thomeer shapes are very practical for application to general geological porous media. The general Thomeer hyperbolic B_ν-curve is not a step function; instead it exhibits a more gradual rate of pore filling, as reflected by the green curves in Figs. 4 and 5. The shape and position of one Thomeer hyperbola reflects the attributes of that single pore system. A typical complex multi-modal Arab D limestone sample can require up to three Thomeer hyperbolas (Clerke et al., 2008). Thomeer (1960) developed an empirical formula for the fractional bulk volume occupied by mercury, which captured the reservoir experimental data behavior:

$$B_\nu(P) = \begin{cases} B_\nu^\infty \exp\left[\frac{-G}{\log(P)-\log(P_d)}\right]; & P > P_d \\ 0; & P \le P_d \end{cases} \tag{22}$$

where P is the pressure applied using the mercury; P_d is the minimum entry pressure, i.e. $B_\nu(P<P_d)=0$. G is the pore geometrical factor, determining the amount of curvature of the hyperbola and B_ν^∞ is the fractional bulk volume reached at infinite pressure. The B_ν^∞ should be identical to the rock's porosity, but in practice it differs by a small factor, $B_\nu^\infty \approx \phi$.

Many examples of fitting the Thomeer function to carbonate MICP measurements can be found in the GeoArabia publication of Clerke et al. (2008).

In the Q-domain, the Thomeer function (Eq. (22)) transforms into

$$B_\nu^Q(Q) = \begin{cases} B_\nu^\infty \exp\left[\frac{-g}{Q-Q_d}\right]; & Q > Q_d \\ 0; & Q \le Q_d \end{cases} \tag{23}$$

where $Q=\ln(P)$; $Q_d=\ln(P_d)$ and $g=\ln(10)G=2.3G$.

Inserting these expressions into the incomplete Laplace transformation of Eq. (17) with the change of variable to $y=Q-Q_d$ yields

$$\tilde{B}_\nu^Q(2D_\lambda) = B_\nu^\infty e^{-2D_\lambda Q_d} \int_{y=0}^{\infty} e^{-g/y} e^{-2D_\lambda y}\, dy \tag{24}$$

By introducing $x=D_\lambda y$ one obtains

$$\tilde{B}_\nu^Q(2D_\lambda) = B_\nu^\infty e^{-2D_\lambda Q_d} \frac{1}{D_\lambda} \int_{x=0}^{\infty} e^{-g'/x} e^{-2x}\, dx = \frac{1}{2D_\lambda} B_\nu^\infty e^{-2D_\lambda Q_d} \sqrt{8g'} K_1(8g') \tag{25}$$

where $g'=D_\lambda g$ and K_1 is the modified Bessel function of the second kind (Abramowitz and Stegun) of order 1.

The permeability expression of Eq. (19) then reads

$$\kappa = \frac{\xi^2}{8} B_\nu^\infty e^{-2Q_d} \left(\frac{L}{L_d}\right)^2 \sqrt{8g'} K_1(8g') \tag{26}$$

where $g' = D_\lambda g$ and $\xi \approx 107\ \mu m$ psi.

All of the relative tortuosity effects associated with D_λ and g' are contained in the expression $\sqrt{8g'}K_1(8g')$!

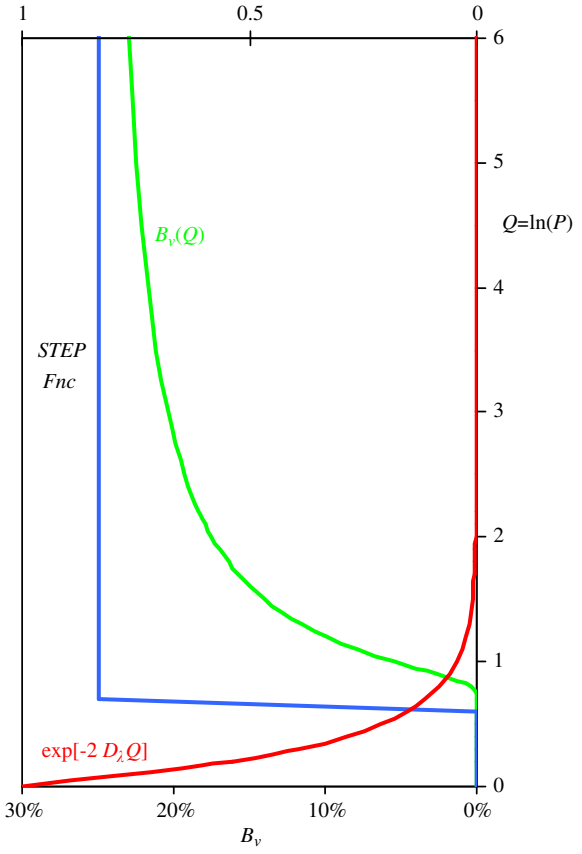

Fig. 5. Laplace transform of two B_v curves, i.e. an artificial step function (blue) and a realistic B_v shape (green). (For interpretation of the references to color in this figure legend, the reader is referred to the web version of this article.)

Eq. (26) expresses the single Thomeer pore system permeability in the Q-domain. Alternate expressions are

- In terms of entry mercury pressure, P_d :

$$\kappa = \frac{\xi^2}{8}\frac{B_v^\infty}{P_d^2}\left(\frac{L}{L_d}\right)^2\sqrt{8g'}K_1(8g') \tag{27}$$

- In terms of the maximum pore throat diameter, r_d :

$$\kappa = \frac{1}{8}r_d^2 B_v^\infty\left(\frac{L}{L_d}\right)^2\sqrt{8g'}K_1(8g') \tag{28}$$

when comparing this equation with the earlier general result (Eq. (9)), $\kappa = \frac{1}{8}r_d^2\phi(L/L_d)^2\langle\chi_L^2\rangle$ it can be seen that $\langle\chi_L^2\rangle \equiv \sqrt{8g'}K_1(8g')$. In the limiting case for very small g's, the B_v curve approaches a simple step function, and $\lim_{g\to 0}\sqrt{8g'}K_1(8g') = 1$. Eq. (28) thus leads to Eq. (21).

5.1. Modified Bessel function—a practical approximation

The modified Bessel function of the second kind $K_1(y)$ is important for the general permeability representations (Eqs. (26)–(28)) when applying the Laplace transform to the Thomeer function. The modified Bessel function is not easy to calculate, but approximations are known for certain parameter ranges. The normal range of variation[1] for the Thomeer G is between 0.2 and 1.5, and therefore $g=2.3G$ is between 0.5 and 4 and $y=\sqrt{8g}$ is in the range, 2–5.6. For this range of argument, the $yK_1(y)$ is well approximated by the simple exponential:

$$yK_1(y) \approx \sqrt{2}e^{-0.828y} \tag{29}$$

In Fig. 6 the two expressions in Eq. (29) are compared. The match for $0.8 < y < 5$ is excellent.

With the approximation of Eq. (29), the permeability of a single pore system described by a general Thomeer hyperbola is

in terms of the maximum pore throat diameter, r_d :

$$\kappa \approx \frac{1}{4\sqrt{2}}r_d^2 B_v^\infty\left(\frac{L}{L_d}\right)^2 e^{-3.55\sqrt{D_\lambda G}}; \tag{30}$$

in the convenient mathematical Q–domain :

$$\kappa \approx \frac{\xi^2}{4\sqrt{2}}B_v^\infty e^{-2Q_d}\left(\frac{L}{L_d}\right)^2 e^{-2.34\sqrt{D_\lambda g}} \quad \text{and} \tag{31}$$

in terms of the entry mercury pressure, P_d :

$$\kappa \approx \frac{\xi^2}{4\sqrt{2}}\frac{B_v^\infty}{P_d^2}\left(\frac{L}{L_d}\right)^2 e^{-3.55\sqrt{D_\lambda G}} \tag{32}$$

These formulae can be used to calculate permeability for any source of appropriate pore architecture data at any consistent scale.

Filling in the constant $\xi \approx 107\ \mu m$ psi and using the fact that 1 Darcy$\equiv$(1 μm)^2 the permeability of Eq. (32) can be written as

$$\kappa \approx 2024\frac{B_v^\infty}{P_d^2}\left(\frac{L}{L_d}\right)^2 e^{-3.55\sqrt{D_\lambda G}}, \tag{33}$$

where κ is in Darcy; B_v^∞ is in fractions; P_d is in psi.

Eq. (33) allows for the calculation of permeability from porosimetry data expressed in the Thomeer form without adjustable parameters and without data fitting. The values, L/L_d and D_λ are global parameters determined by the topology of the fractal pore geometry. Individual sample behavior enters through the three parameters defining the Thomeer hyperbola. This result only applies for the simple monomodal pore system. The exponents on the variables in our permeability formula demonstrate the significant shift in emphasis from porosity to the diameter of the largest connected pore throats r_d, and thus P_d. The approximately equal sign is used here only because of the practical approximation used for the modified Bessel function.

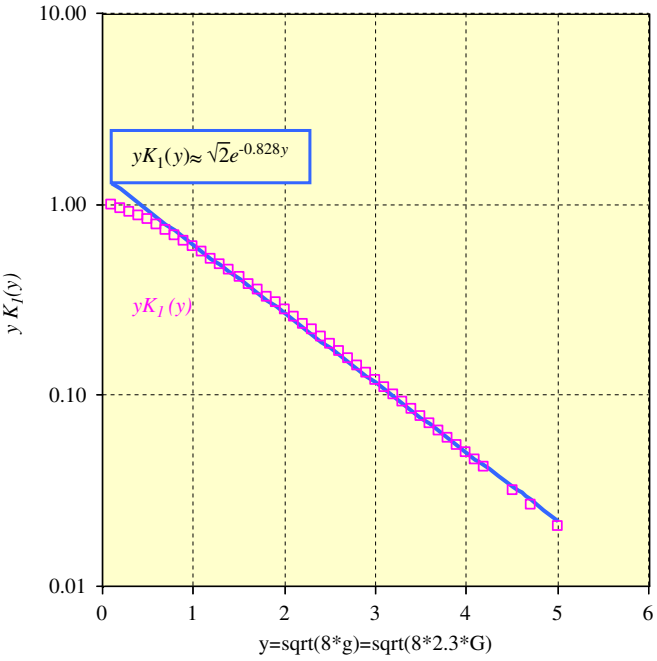

Fig. 6. Simple approximation of $yK_1(y)$ valid for the realistic range of G values.

5.2. Validation test

The validity of Eq. (33) is evaluated using Saudi Aramco's Rosetta Stone (Clerke et al., 2008) data set for the highly connected pore systems of the Arab-D limestone of the Ghawar field. This data set contains data from more than 500 core-plugs all with MICP data analyzed by the Thomeer method and data with porosity and permeability measurements. Much of the sample data required multiple Thomeer hyperbolas (multimodal) which define both macropores and micropores.

The porosity–permeability cross-plot of that data (Clerke et al., 2008) is reproduced in Fig. 7. The correlation between porosity and permeability is poor, normal for carbonate rocks. Additional pore system properties such as largest connected pore-throat diameter are needed to accurately describe this carbonate's permeability (Clerke et al., 2008; Clerke, 2009). This important conclusion is expressed in Eqs.(32) and (33), where the P_d parameter plays the largest role. For proper test of the new formula, it is necessary to eliminate the influence of the micropore system. For that end, we concentrated on primarily monomodal core-plugs and permeabilities of 0.01 md or higher. About 350 core plugs qualified.

The monomodal equation can be applied without any problems to our multimodal system because the micropore system within the Arab-D carbonates contributes very little to the absolute permeability (Clerke et al., 2008). The explanation for this was explored in the discussion surrounding Fig. 4 where the good and poor rock MICP curves are compared. For reservoir carbonates containing macropores along with a form of microporosity, Clerke et al. (2008) and Clerke (2009) showed that the macropores controlled 99.98% of the permeability. However, Eq. (33) can readily be generalized to include micropore permeability corrections.

Regardless of the dominance of the macropores on permeability, the macropore porosity and not the total porosity must be used to test our equation. That means that in testing the permeability equation we must use only the measured data for the macropore system architecture, namely

$$\kappa \approx 2024 \frac{B_{v,1}^{\infty}}{P_{d,1}^2} \left(\frac{L}{L_{d,1}}\right)^2 e^{-3.55\sqrt{D_\lambda G_1}} \tag{34}$$

The insertion of the subscript 1 indicates that we test the formula using the largest pore throat system present in our multimodal samples (usually the macropore system). Note that $B_{v,1}^{\infty} \approx \phi_1$, the porosity of the first pore system, commonly macropores.

For our Arab-D carbonate pore systems we anticipate a Manhattan type percolation length ratio of 2, i.e. $L_d/L \approx 2$, as is argued in the paragraph below Eq. (15) and is illustrated in Fig. 3. Moreover, we believe that the narrow tubular flow paths are very complex linear features in 3 dimensions and are very much like artery systems in human bodies such as the ones seen in lungs. Arteries can have very high fractal dimension, which we take as applicable to carbonate pore systems, i.e. $D_\lambda \approx 1.62$ (Boxt et al., 1994). These two assumptions, i.e. $L_d/L \approx 2$ and $D_\lambda \approx 1.62$, already yield a very good match with the experimental results. When numerical fitting these two global values, we find only slightly different value for the fractal dimension, i.e. $D_\lambda = 1.56$. This D_λ value is consistent with the other determinations of the fractal dimension of tortuous flow paths such as arteries and is nearly identical to the dimension of the self-avoiding random walk (Feder, 1988).

Using the best values for L_d/L (=2) and D_λ (=1.56), Eq. (34) can be written for a monomodal pore system (single Thomeer hyperbola) as

$$\kappa \approx 506 \frac{B_{v,1}^{\infty}}{P_{d,1}^2} e^{-4.43\sqrt{G_1}} \tag{35}$$

where κ is in Darcy, $B_{v,1}^{\infty}$ in fractions and $P_{d,1}$ in psi.

Fig. 8 displays the measured core permeabilities (κ_{core}) against the results of Eq. (35) (κ_{calc}) in cross plot. The match is excellent.

6. Comparison to empirical permeability formulae of Thomeer and Swanson

Our mathematically derived permeability formulas (Eqs. (33) and (35)) must be compared to the empirical derivations of Thomeer (1983) and Swanson (1981) as used widely in the

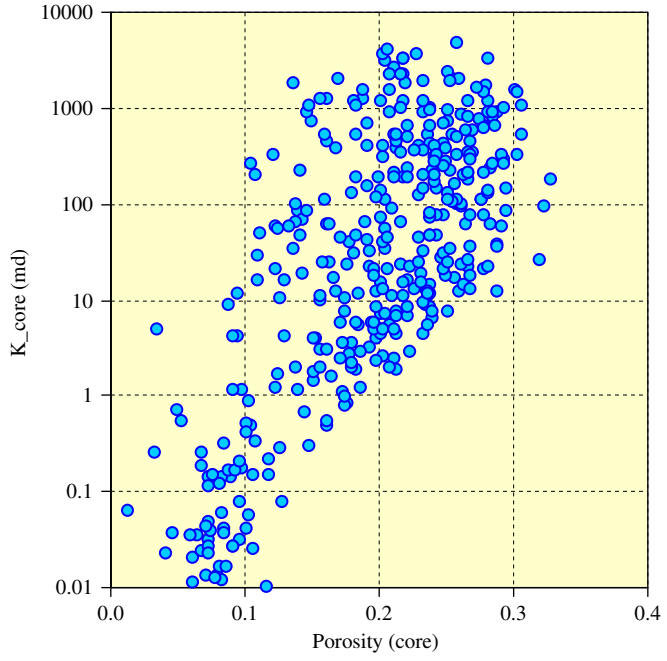

Fig. 7. Cross plot of measured porosity–permeability values for 350 core-plugs of the Arab-D formation in Ghawar.

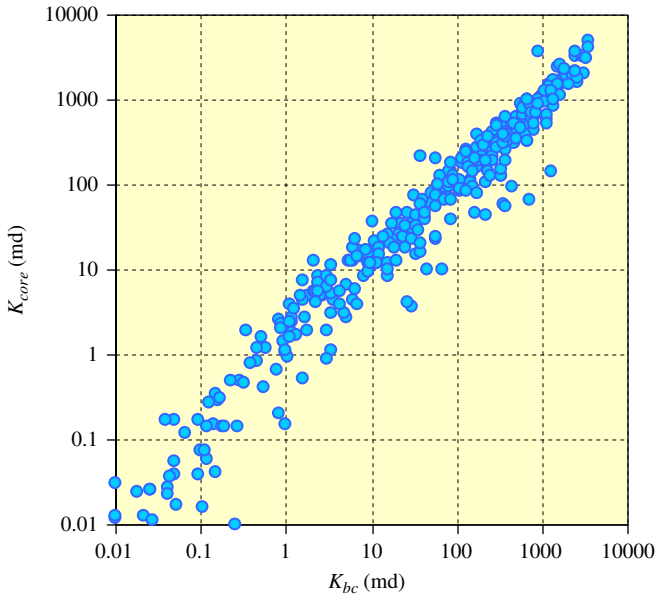

Fig. 8. Comparing the measure Arab-D core plug permeabilities with our calculated ones. The match is excellent.

industry, i.e.

$$\text{Thomeer}: \quad \kappa_{Thm} \approx \alpha \left(\frac{B_v^\infty}{P_d}\right)^2 G^{-\beta} \tag{36a}$$

$$\text{Swanson}: \quad \kappa_{Sw} \approx \alpha \left[\frac{B_v(P)}{P}\bigg|_{max}\right]^\beta \tag{36b}$$

where κ_{Thm} and κ_{Sw} in Darcy, B_v^∞ and B_v are fractional bulk volume, as defined before. P_d is the minimum entry pressure and P is the applied mercury pressure, both in psi. The parameters α and β are empirical fitting parameters, which are obviously different for both expressions.

Fitting the Thomeer permeability of Eq. (36a) to the Shell rock catalog MICP data, Thomeer (1983) proposed $\alpha = 38.1$ and $\beta = 1.334$ for air permeability, which leads to a 1.8 multiplicative uncertainty for the calculated values compared to the actual ones.

Through matching his Eq. (36b) against actual MICP and air permeability measurements on both carbonates and clastics, Swanson obtained fitting parameters $\beta \approx 1.691$ and $\alpha \approx 962$. Note that the original Swanson (1981) α-value, 399, is for κ in md and B_v in %. We have to convert these to our units, i.e. for κ in Darcy and B_v in fractions. Then the value for α is obtained as follows: $962 = (399 \times 100^{1.691})/1000$.

The Thomeer and Swanson permeability formulae share a similar form but show an important difference compared to our expression (Eq. (35)). In both Thomeer and Swanson equations, it is assumed that the B_v^∞ and the P_d share the same exponent, i.e. 2 in case of κ_{Thm} and β (1.69) in case of κ_{Sw}. This cannot be supported from a physics point of view (as can be seen in Appendix A). The maximum pore throat diameter, or minimum entry pressure P_d, plays a stronger role than the pore system volume B_v^∞ or ϕ.

6.1. Thomeer

For comparison to Thomeer, we start with our permeability formula (Eq. (35)), with the macro-pore index removed:

$$\kappa_{bc} \approx 506 \frac{B_v^\infty}{P_d^2} e^{-4.43\sqrt{G}} \tag{37}$$

Equating the Thomeer permeability of Eq. (36a) to our expression (Eq. (37)) it is possible to find the comparative values for α and β, consistent with our formulation, i.e.

$$\kappa_{Thm} \approx \kappa_{bc} \Rightarrow \ln(\alpha) \approx \ln(G)\beta + \ln(\kappa_{bc}) - 2\ln\left(\frac{B_v^\infty}{P_d}\right) \tag{38}$$

This must hold for all possible pore system Thomeer parameters and thus defines a suite of lines in the $\ln(\alpha)$–β plane. For the sake of simplicity Eq. (38) it can be written as

$$\ln(\alpha) \approx a\beta + b, \text{ where } a = \ln(G) \text{ and } b = \ln(\kappa_{bc}) - 2\ln\left(\frac{B_v^\infty}{P_d}\right) \tag{39}$$

Using our 350 carbonate plug measurements, a and b values for the carbonate core plugs can be calculated. The result is shown in Fig. 9, where a and b are shown in cross plot. A good correlation can be seen and an approximate linear relationship between these two parameters can be established as

$$b \approx -1.40a + 3.93 \tag{40}$$

If Eq. (38) is valid then all the lines defined by Eq. (39) should pass roughly through one point in the $\ln(\alpha)$–β plane, i.e. through point $[\ln(\alpha_o), \beta_o]$ and thus

$$\ln(\alpha_o) \approx a\,\beta_o + b,$$

for all a and b values on the red line in Fig. 9. (41)

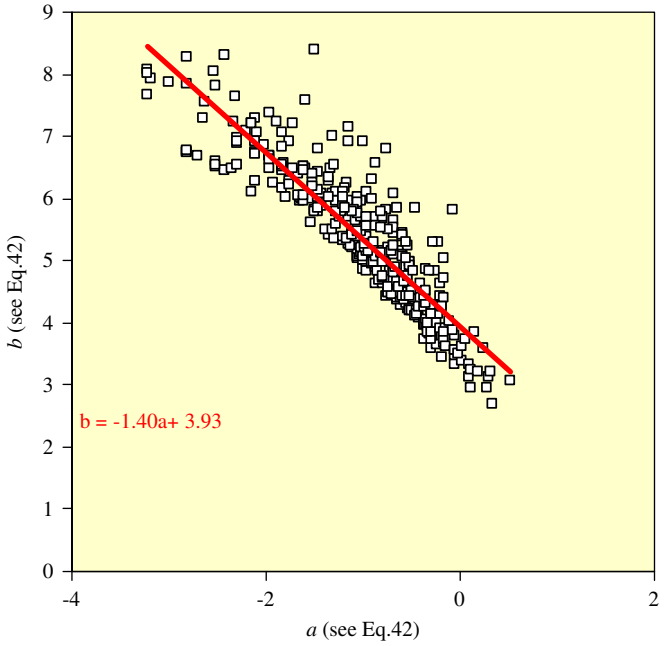

Fig. 9. Correlation cross plot between values a and b of Eq. (39) for Thomeer empirical parameters.

Since α_o should be independent of a, than $\partial/\partial a \ln(\alpha_o) = 0$ and thus

$$\beta_o + \frac{\partial b}{\partial a} \approx 0 \quad \text{or} \quad \beta_o \approx -\frac{\partial b}{\partial a} \tag{42}$$

Using Eqs. (40) and (42) the new empirical values are $\beta_o \approx 1.40$ and $\alpha_o \approx 50.9$. These are different than the original values found by Thomeer, 1.334 and 38.1, respectively, but not by a great amount.

In Fig. 10 our calculated permeabilities κ_{bc} are compared to the Thomeer results, κ_{Thm}, using the new parameters $\beta_o \approx 1.40$ and $\alpha_o \approx 50.9$ for our data. The correlation is very good, indicating that both formulas are comparable. In the region below 1 md (low porosity and permeabilities), a deviation from the linear trend can be observed and our permeabilities are slightly higher than what the Thomeer formula predicts. Probably, the quadratic porosity dependence in Thomeer's equation, produces a reduction of the permeability at low porosity values. The Thomeer formulation deviates from our own calculation at low porosities and permeabilities and from actual permeability data at low permeabilities (Clerke et al., 2008). The empirical relationship derived by Thomeer is excellent and comparable to the one derived here, but it assumes a quadratic porosity dependence which is noticeably different from our result.

6.2. Swanson

At least as successful as Thomeer's permeability is Swanson's formula (Swanson, 1981) of Eq. (36b). It is computed using MICP parameters related to the maximum value of the ratio between the fractional bulk volume occupied by mercury B_v and the applied mercury pressure P, i.e. B_v/P.

Let the maximum of the ratio $B_v(P)/P$ occur at a certain mercury pressure P_{Sw}. Assuming that the fractional bulk volume occupied $B_v(P)$ is well described by the Thomeer hyperbola (Eq. (22)), the Swanson pressure can be derived, i.e. $P_{sw} = P_d \exp(\sqrt{g})$, where P_d is the minimum entry pressure and $g = 2.3\,G$. Using this result, Swanson's permeability of Eq. (36b) can be analytically rewritten as

$$\kappa_{Sw} \approx \alpha \left[\frac{B_v^\infty}{P_d} e^{-2\sqrt{g}}\right]^\beta \tag{43}$$

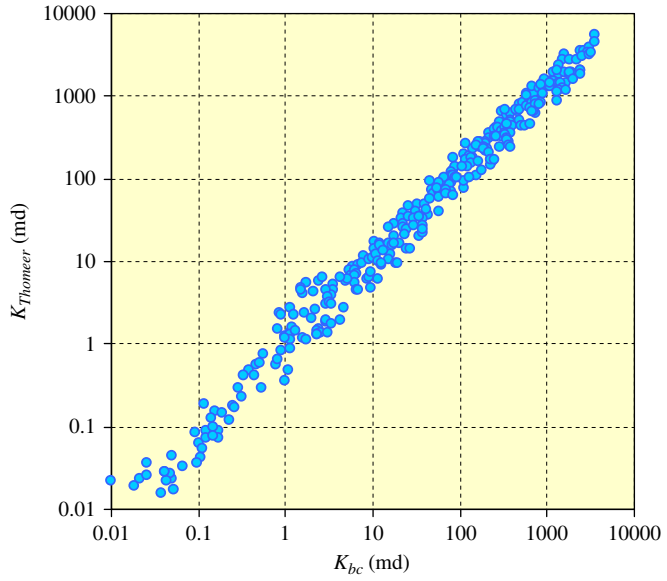

Fig. 10. Comparing Thomeer's empirical permeability with the permeability derived in this paper.

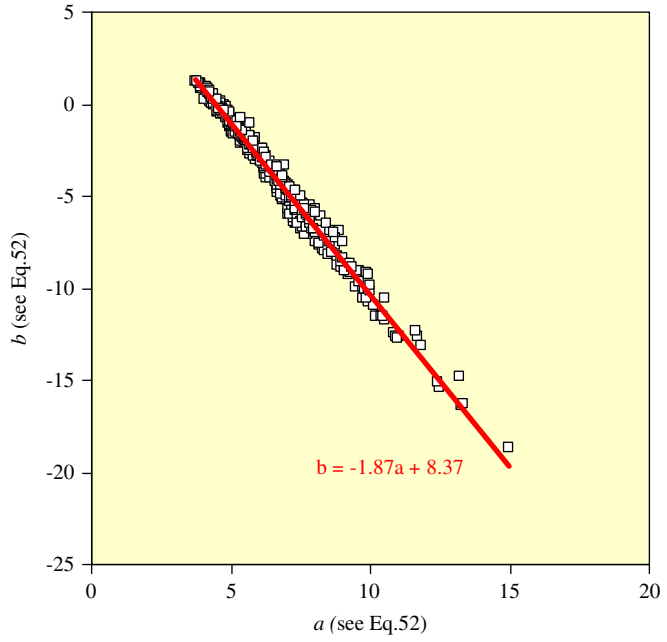

Fig. 11. Correlation cross plot between values a and b of Eq. (45) for Swanson's empirical parameters.

Following the same arguments used for the Thomeer permeability in the previous section, we derive Swanson's α and β values consistent with our carbonate data and our permeability formula. Along the same line of reasoning which leads to Eqs. (38) and (39), it can be said that

$$\kappa_{Sw} \approx \kappa_{bc} \Rightarrow \ln(\alpha) \approx a\beta + b \tag{44}$$

$$\text{where } a = -\ln\left[\frac{B_v^{\infty}}{P_d} e^{-2\sqrt{g}}\right] \quad \text{and} \quad b = \ln(\kappa_{bc}) \tag{45}$$

This must hold for all possible rock (Thomeer) parameter values. Eq. (44) defines a suite of lines in the $\ln(\alpha)$–β plane.

From our 350 carbonate measurements and using Eq. (45), a and b values for the carbonate core plugs can be calculated. The result is shown in Fig. 11, for a and b in cross plot. An excellent linear relationship is observed, much better than the one derived from κ_{Thm} as shown in Fig. 9, i.e.

$$b \approx -1.87a + 8.37 \tag{46}$$

If Eq. (44) is valid then all the lines defined by Eq. (44) should roughly pass through one point in the $\ln(\alpha)$–β plane, i.e. through point $[\ln(\alpha_o), \beta_o]$ and thus:

$$\ln(\alpha_o) \approx a\beta_o + b$$

or all a and b values on the red line in Fig.11. (47)

$$\text{Then } \frac{\partial}{\partial a}\ln(\alpha_o) = 0 \quad \text{and} \quad \beta_o + \frac{\partial b}{\partial a} \approx 0 \quad \text{or} \quad \beta_o \approx -\frac{\partial b}{\partial a} \tag{48}$$

Using Eqs. (46) and (47), we obtain the new Swanson empirical values as $\beta_o \approx$ 1.87 and $\alpha_o \approx$4316, which are considerably different than the ones original proposed by Swanson, i.e. 1.691 and 962 respectively.

Applying the new values gives the following alternative Swanson permeability expression

$$\kappa_{sw} \approx 4316\left(\frac{B_v^{\infty}}{P_d}\right)^{1.87} e^{-5.67\sqrt{G}} \tag{49}$$

This expression matches well with the permeabilities computed from our new formulation as shown in Fig. 12.

Note that the expressions for κ_{Sw} (Eq. (49)) and κ_{Thm} (Eq. (36a)) share a comparable power law for the (B_v^{∞}/P_d) term (1.87 and 2.0 respectively), only the G term is different. However, the G term used by Swanson has the $\sqrt{G}$ in the exponential, like our expression. In both formulae the exponential G term is smaller than 1, reducing the permeability with increasing G. This makes sense because larger G values mean more pore throat variability within the pore system and thus lower permeability.

6.3. Leverett J Function

Both Thomeer and Swanson proposed a nearly quadratic dependence for the porosity term, B_v^{∞} or ϕ, in their empirical permeability formulae yet a common industry saturation-height model approach for simple pore systems often uses the Leverett J function $\sqrt{\kappa/\phi}$ scaling relationship (Amyx et al., 1960). Our

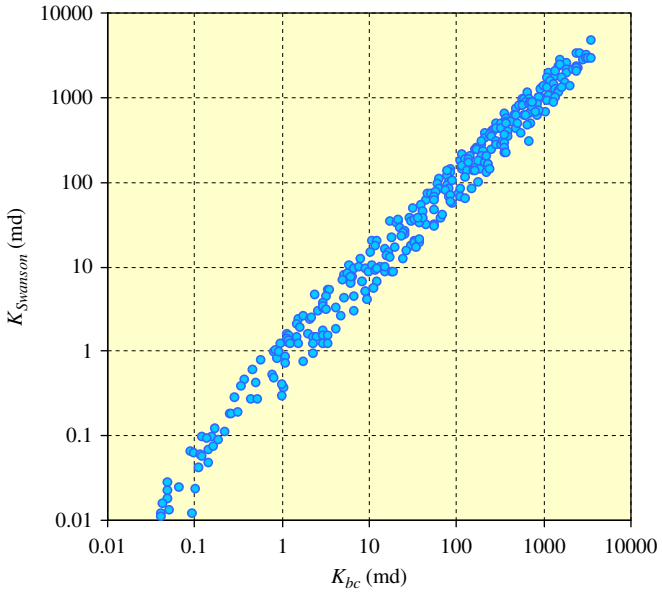

Fig. 12. Comparing the empirical Swanson permeabilities with our calculated ones.

formulation, which is linear in the porosity term, shows the clear advantage given by the $\sqrt{\kappa/\phi}$ parameterization of Leverett for a *monomodal* pore system. Using the formulation of Eq. 35 and equating B_v^∞ and ϕ, the Leverett approach yields

$$\sqrt{\frac{\kappa}{\phi}} \approx \frac{22.5}{P_d} e^{-2.22\sqrt{G}} \tag{50}$$

Completely removing the porosity dependence and creating a modified relationship to P_d and G only. For porous media that are monomodal and exhibit small variations in G values, the $\sqrt{\kappa/\phi}$ scaling is nearly equivalent to using a $1/P_d$ form!

7. Conclusions

Detailed studies using high quality measurements of the pore systems of Arab D limestone (Clerke et al., 2008) demonstrate the inadequacy of porosity–permeability transforms for complex carbonates and problems with the Thomeer permeability calculation for permeabilities less than 10 md (figure 19 in Clerke et al., 2008). That study generated a wealth of complete porosimetry information in the form of Thomeer analyzed MICP data and demonstrated the importance of the largest connected pore throat diameter in the permeability calculation (Clerke et al., 2008, Clerke, 2009). Combined, these observations motivated a renewed interest in the capacity to improve the calculation of permeability from porosimetry data as originally demonstrated by Purcell (1949).

This work extends those early empirical efforts by rigorously developing a fractally tortuous tubular bundle. The results use a practical fractal conceptual model which relates the tube radii to the tube lengths. A simple percolation model for a highly connected system sets the ratio between the length of the largest diameter tube and the sample length. The result is a closed form solution for the permeability from porosimetry with no adjustable parameters. When applied to mercury porosimetry data, the approach is shown to be equivalent to the operation of an incomplete Laplace transform upon the porosimetry data.

Practicality is further extended using explicit expressions for the results when the porosimetry data is monomodal and expressed in the well-known Thomeer form. The general result derived here utilizes the modified Bessel function of the second kind. An even more practical expression employs an approximation for the modified Bessel function, giving a form easily used for real geologic porous media still without adjustable parameters.

To validate and emphasize the utility of this new formulation, without adjustable parameters; we compare the calculations to our extensive set of carbonate porosimetry data[1], with excellent results from 5000 md to 0.1 md.

The exponents in our new formula demonstrate a significant shift in emphasis from previous efforts, from porosity to the diameter of the largest connected pore throats, P_d, as the major control on permeability. Our result is shown to be consistent with previous empirical formulae of Thomeer (1983) and Swanson (1981) and yet also explains the applicability of the Leverett J function to monomodal pore systems.

Importantly, and in contrast to previous empirical permeability models, this new mathematical formulation sets the stage for a complete and scale independent understanding of permeability in multimodal carbonate pore systems commonly encountered in the Arab D limestone and in other geological porous media.

Acknowledgments

We would like to thank our colleagues Denis Schmitt and Jim Funk for their willingness and perseverance to thoroughly review the text and mathematics. We are also thankful to the Reservoir Characterization Department of Saudi Aramco for continued support and the Saudi Aramco management—for permission to publish this work.

Appendix A. Derivation of tubular permeability

In this appendix the permeability of rock will be derived by representing its pore system by an assortment of all kind of different tubes, connecting one end of the rock to the other. This argumentation follows the ideas of Purcell (1949) and Burdine (1953). It is assumed that the tubes are embedded in a solid rock sample of length L. The tubes have variable lengths L_i, all longer than the length of the rock sample, i.e. $L_i > L$.

The Hagen–Poiseuille equation has now its most general form:

$$\frac{dV_{liq}}{dt} = \sum_i n_i \frac{\pi r_i^4}{8\mu L_i} \Delta P \tag{A1}$$

Solving the permeability yields:

$$\kappa = \frac{1}{8}\sum_i n_i \frac{\pi r_i^4}{A}\frac{L}{L_i} = \frac{1}{8}\sum_i \underbrace{\frac{n_i \pi r_i^2 L_i}{AL}}_{\Delta\varphi_i}\left(\frac{L}{L_i}\right)^2 r_i^2 \Leftrightarrow \kappa = \frac{1}{8}\sum_i \Delta\varphi_i r_i^2 \left(\frac{L}{L_i}\right)^2 \tag{A2}$$

where $\Delta\varphi_i$ is the porosity related to the pore volume behind all pore throats with radius r_i and is an incremental step in the build up towards the total porosity. As explained in Appendix B it is similar to the fractional bulk volume of mercury injected into the sample during an MICP experiment, i.e. $\Delta\varphi_i \equiv \Delta B_{v,i}$. Of course $\sum_i \Delta\varphi_i = \phi$, i.e. the total porosity.

Note that in case L_i is slowly varying as a function of i (or r_i). Normalizing to the bulk porosity and the largest pore-throat radius, yields:

$$\kappa = \frac{1}{8} r_d^2 \phi \sum_i \frac{\Delta\varphi_i}{\phi}\left(\frac{r_i}{r_d}\right)^2 \left(\frac{L}{L_i}\right)^2 \tag{A3}$$

The lengths of the tubes, L_i, in this equation are compared to the length of the piece of rock, i.e. L. Now the comparison with the length of the sample is replaced by the comparison with the length of the tube with radius r_d, which is assumed to have the shortest length L_d, that is smaller than L_i, and larger than the length of the rock-tube ensemble (i.e. the length of the sample or core-plug, L).

$$\kappa = \frac{1}{8} r_d^2 \phi \sum_i \frac{\Delta\varphi_i}{\phi}\left(\frac{r_i}{r_d}\right)^2 \left(\frac{L}{L_i}\right)^2 \left(\frac{L_d}{L_d}\right)^2 \Leftrightarrow \kappa = \frac{1}{8} r_d^2 \phi \left(\frac{L}{L_d}\right)^2 \sum_i \frac{\Delta\varphi_i}{\phi}\left(\frac{r_i}{r_d}\right)^2 \left(\frac{L_d}{L_i}\right)^2 \tag{A4}$$

Appendix B. Permeability as a Laplace transform

This derivation starts with the general result of Eq. 15, which after some rearranging can be written as

$$\kappa = \frac{1}{8} r_d^{2(1-D_\lambda)} \left(\frac{L}{L_d}\right)^2 \sum_i \Delta\varphi_i r_i^{2D_\lambda} \tag{B1}$$

By choice the summation starts with the largest diameter tube going downwards, i.e. $r_1 \equiv r_d$ and $r_{i+1} < r_i$, with $\lim_{i\to\infty} r_i = 0$ The reason for this is that in a later stage of the derivation we will change from pore-throat radii as key variable to entry pressures, which are inversely proportional to the radii (see Eq. (B10)). $\Delta\varphi_i$ is the porosity associated with all the tubes with radii r_i. The sum of all tubular porosities is the total bulk porosity, i.e. $\sum_i \Delta\varphi_i = \phi$. The

partial sum is defined as

$$\varphi_N = \sum_{i=1}^{N} \Delta\varphi_i \equiv \varphi(r_N) \tag{B2a}$$

The variable φ_N is the cumulative porosity of all the tubes with radii *larger* than r_N (and smaller than r_d). Note that $\lim_{N\to\infty} \varphi_N = \phi$. The continuous equivalent of discrete expression of Eq. (B2a) is

$$\varphi = \int_0^{\varphi} d\varphi \quad \text{or} \quad \varphi(r) = \int_r^{r_d} \frac{d\varphi}{dr} dr. \tag{B2b}$$

Note that $\int_{\varphi=0}^{\phi} d\varphi = \int_0^{r_d} (d\varphi/dr) dr = \phi$, which is the bulk porosity.

From Eq. (B2b) it can be understood that $\varphi(r)$ is monotonically decreasing with increasing r as can be seen. Moreover, $\varphi(0) = \phi$ and $\varphi(r_d) = 0$. This implies that the inverse of this function, i.e. $r(\varphi)$is monotonically decreasing with increasing φ, with $r(0) = r_d$ and $r(\phi) = 0$.

In the continuous limit the summation of Eq. B1 can be replaced by an integral:

$$\kappa = \frac{1}{8} r_d^{2(1-D_\lambda)} \left(\frac{L}{L_d}\right)^2 \int_{\varphi=0}^{\phi} d\varphi\, r^{2D_\lambda} \tag{B3}$$

Note that when $\varphi \to 0$then$r \to r_d$ and $\varphi \to \phi$for$r \to 0$.

Intermezzo: The link to Purcell's approach

Let us assume that $D_\lambda = 1$ (no tortuosity), then the integral of Eq. (B3) looks like $\int_{\varphi=0}^{\phi} d\varphi r^2$ or $\phi \int_{\varphi=0}^{\phi} (d\varphi/\phi) r^2$. Since $\frac{\varphi}{\phi} \equiv S$ is the saturation of the non-wetting liquid, i.e. mercury, the integral becomes $\phi \int_{S=0}^{1} dS\, r^2$. As we will see $r \propto 1/P_c$, where P_c is the mercury entry pressure and thus $\phi \int_{S=0}^{1} dS\, r^2 = \phi \int_{S=0}^{1} dS/P_c^2$ which is the same integral expression as part of the permeability formula proposed by Purcell (1949).

From here onwards let us concentrate on the integral $\int_{\varphi=0}^{\phi} d\varphi\, r^{2D_\lambda}$, which is part of Eq. (B3).

Using $\int df\, g = fg - \int f\, dg$, one obtains

$$\int_{\varphi=0}^{\phi} d\varphi\, r^{2D_\lambda} = \varphi\, r^{2D_\lambda}\Big|_{\varphi=0}^{\varphi=\phi} - 2D_\lambda \int_{r=r_d}^{0} \varphi\, r^{2D_\lambda - 1}\, dr \tag{B4}$$

Note that when $\varphi = 0$ then $\varphi\, r^{2D_\lambda} = 0$, since $r \le r_d$. Moreover, since $\varphi(r)$ is the cumulative porosity for all radii between r and r_d it can be seen that $\lim_{\varphi\to\phi} r = 0$, and thus $\lim_{\varphi\to\phi} \varphi r^{2D_\lambda} = 0$. Therefore the first term on the right hand side of Eq. (B4) is zero and thus

$$\int_{\varphi=0}^{\phi} d\varphi\, r^{2D_\lambda} = 2D_\lambda \int_{r=0}^{r_d} \varphi(r)\, r^{2D_\lambda - 1}\, dr \tag{B5}$$

Eq. (B3) thus becomes

$$\kappa = \frac{1}{4} D_\lambda r_d^{2(1-D_\lambda)} \left(\frac{L}{L_d}\right)^2 \int_{r=0}^{r_d} \varphi(r) r^{2D_\lambda - 1}\, dr = \frac{1}{4} D_\lambda\, r_d^2 \left(\frac{L}{L_d}\right)^2 \int_{r=0}^{r_d} \varphi(r) \left(\frac{r}{r_d}\right)^{2D_\lambda - 1} \frac{dr}{r_d} \tag{B6}$$

$$\text{Now change variable}: \; y = -\ln\left(\frac{r}{r_d}\right) \Leftrightarrow \frac{r}{r_d} = e^{-y} \quad \text{and} \quad \frac{dr}{r_d} = -e^{-y}\, dy, \tag{B7}$$

then Eq. (B6) becomes

$$\kappa = \frac{1}{4} D_\lambda r_d^2 \left(\frac{L}{L_d}\right)^2 \int_{y=\infty}^{y=0} \varphi(r_d e^{-y}) e^{(1-2D_\lambda)y} (-e^{-y}\, dy)$$

$$\Rightarrow \kappa = \frac{1}{4} D_\lambda r_d^2 \left(\frac{L}{L_d}\right)^2 \underbrace{\int_{y=0}^{\infty} \varphi_y(y) e^{-2D_\lambda y}\, dy}_{\text{Laplacetransform}} \tag{B8}$$

The integral in this expression is the Laplace transform of φ in the y-domain. In abbreviated form the permeability can be expressed as:

$$\kappa = \frac{1}{4} D_\lambda r_d^2 \left(\frac{L}{L_d}\right)^2 \hat{\varphi}_y(2D_\lambda) \tag{B9}$$

The symbol ^ indicates that it is a Laplace transform. The subscript y indicates that the transform is in the y-domain.

So in short: the permeability of a porous rock whose pore system is well modeled with a tubular bundle can be expressed as the Laplace transform of the cumulative porosity function in the y-domain (Eq. (B8)).

The cumulative porosity φ for a tubular pore system is the same as the fractional bulk volume occupied with mercury B_v in an MICP experiment. As the pressure P increases the tubes will be gradually filled with mercury, starting with the largest diameter tube(s), having the largest radius r_d. The pressure related to that entrance is P_d, the minimum entry pressure, i.e. none of the tubes or pores are filled for mercury pressure less than P_d. Each tube of radius r has its characteristic entry pressure P, i.e.

$$P \approx \frac{2}{r} [\sigma \cos(\theta)]_{Hg-Air} \equiv \frac{\xi}{r} \tag{B10}$$

Note that when r is in μm and P in psi then $\xi \approx 107$ psi μm (for round tubes/pore throats), since

$$\xi = 2[\sigma \cos(\theta)]_{Hg-Air} \approx 734 \text{ dyn/cm} = 107 \text{ psi } \mu m \tag{B11}$$

The fractional bulk volume occupied B_v is normally given as a function of the applied mercury pressure $B_v(P)$, but with Eq. (B10) it can expressed as a function of the tube radii (or pore-throat radii) as well:

$$B_v(P) = B_v\left(\frac{\xi}{r}\right) \equiv B_v^r(r), \text{ i.e. the } B_v \text{inthe } r\text{–domain}, \tag{B12}$$

which is the fractional bulk volume occupied with mercury at a certain pressures P. This is the same as the fractional volume (read cumulative porosity) of all the tubes with radii greater than r, where $r \approx \xi/P$ (see Eq. (B10)). That means that the B_v in the r-domain is the same as the cumulative porosity, i.e. $B_v^r(r) = \varphi(r)$ and Eq. (B9) can be written as

$$\kappa = \frac{1}{4} D_\lambda r_d^2 \left(\frac{L}{L_d}\right)^2 \hat{B}_v^y(2D_\lambda) \tag{B13}$$

where $\hat{B}_v^y$ is the Laplace transform of B_v in the y-domain.

In the P-domain, using Eq. (B10), one obtains

$$\kappa = \frac{\xi^2}{4} D_\lambda \frac{1}{P_d^2} \left(\frac{L}{L_d}\right)^2 \hat{B}_v^y(2D_\lambda) \tag{B14}$$

For convenience this expression is also given in the Q-domain, where $Q = \ln(P)$, a transformation which will be extensively used here and elsewhere. In the Q-domain, Eq. (B14) reads

$$\kappa = \frac{\xi^2}{4} D_\lambda e^{-2Q_d} \left(\frac{L}{L_d}\right)^2 \hat{B}_v^y(2D_\lambda) \tag{B15}$$

Note that $\hat{B}_v^y(2D_\lambda)$ is just a constant, i.e. the Laplace transform in point $2D_\lambda$.

This number can also be calculated in the Q-domain. For that variable y (Eq. (B7)) has to be expressed in terms of mercury pressure and variable Q:

$$y = -\ln\left(\frac{r}{r_d}\right) \approx \ln\left(\frac{P}{P_d}\right) = Q - Q_d \tag{B16}$$

Then

$$\hat{B}_v^y(2D_\lambda) = \int_{y=0}^{\infty} B_v^y(y) e^{-2D_\lambda y}\, dy = \int_{Q=Q_d}^{\infty} B_v^y(Q-Q_d) e^{-2D_\lambda Q} e^{+2D_\lambda Q_d}\, dQ$$

$$= e^{+2D_\lambda Q_d} \int_{Q=Q_d}^{\infty} B_v^Q(Q) e^{-2D_\lambda Q}\, dQ \equiv \tilde{B}_v^Q(2D_\lambda)$$

So that the permeability becomes

$$\kappa = \tfrac{\xi^2}{4} D_\lambda e^{-2(1-D_\lambda)Q_d} \left(\frac{L}{L_d}\right)^2 \tilde{B}_v^Q(2D_\lambda) \tag{B17}$$

where B_v^Q is B_v in the Q-domain, where $Q=\ln(P)$.

Note that the tilde ~ above the B indicates that it is an *incomplete* Laplace transform, since the integration starts at Q_d rather than 0. However when $Q_d > 0$, this can still be written as a Laplace transform as explained below.

Note that $B_v(P) = B_v^Q(Q) = B_v^y(y)$, because $B_v(P) = B_v(e^Q) \equiv B_v^Q(Q)$
and $B_v(P) = B_v(P_d e^y) \equiv B_v^y(y)$ (B18)

When $P_d > 1$ psi, i.e. $Q_d > 0$

By definition $B_v(P < P_d) = 0$ so $B_v^Q(Q < Q_d) = 0$. When $Q_d > 0$, i.e. when the minimum mercury entry pressure $P_d > 1$ psi (which is normally the case for Arab-D carbonates), the lower integration limit can without problems be extended from Q_d to 0,[1] turning the integral into a Q-domain Laplace transform:

$$\int_{Q=Q_d}^{\infty} B_v^Q(Q) e^{-2D_\lambda Q}\, dQ = \underbrace{\int_{Q=0}^{\infty} B_v^Q(Q) e^{-2D_\lambda Q}\, dQ}_{\text{Laplacetransform}} \quad \text{and} \quad \tilde{B}_v^Q(2D_\lambda) \equiv \hat{B}_v^Q(2D_\lambda) \tag{B19}$$

This means than in these cases (and almost all Arab-D limestones) Eq. (B18) can be expressed as a normal Laplace transform in the Q-domain:

$$\kappa = \frac{\xi^2}{4} D_\lambda e^{-2(1-D_\lambda)Q_d} \left(\frac{L}{L_d}\right)^2 \hat{B}_v^Q(2D_\lambda) \tag{B20}$$

Note that for $D_\lambda = 1$, and $\kappa = \xi^2/4(L/L_d)^2 \hat{B}_v^Q(2)$

References

Abramowitz, Stegun, 1972. Handbook of Mathematical Functions. (Equation.29.3.122). United States Department of Commerce, National Bureau of Standards.

Amyx, Bass, Whiting, 1960. Petroleum Reservoir Engineering. McGraw-Hill Book Company, New York, NY.

Angulo, R.F., Alvarado, V., Gonzalez, H., 1992. Fractal dimensions from mercury intrusion capillary tests. SPE 23695.

Bird, R.B., Stewart, W.E., Lightfoot, E.N., 1960. Transport Phenomena. John Wiley & Sons, New York.

Boxt, L.M., Katz, J., Liebovitch, L.S., Jones, R., Esser, P.D., Reid, L., 1994. Fractal analysis of pulmonary arteries: the fractal dimension is lower in pulmonary hypertension. J. Thorac. Imaging, Winter 9 (1), 8–13.

Burdine, N.T., 1953. Relative permeability calculations from pore size distribution data. Trans. AIME 198, 71–78.

Calhoun, J.C., Lewis, M., Newman, R.C., 1949. Experiments on the capillary properties of porous solids. Trans. AIME 186, 189–196.

Cantrell, D.M., Hagerty, R.M., 1999. Microporosity in Arab D Carbonates, Saudi Arabia. GeoArabia 4 (2), 129–154.

Cantrell, D.M., Hagerty, R.M., 2003. Reservoir rock classification, Arab-D reservoir, Ghawar field, Saudi Arabia. GeoArabia 8 (3), 453–462.

Clerke, E.A., Mueller III, H.W., Phillips, E.C., Eyvazzadeh, R.Y., Jones, D.H., Ramamoorthy, R., Srivastava, A., 2008. Application of Thomeer Hyperbolas to decode the pore systems, facies and reservoir properties of the Upper Jurassic Arab D Limestone, Ghawar field, Saudi Arabia: a Rosetta Stone approach. , GeoArabia 13 (4), 113–160.

Clerke, E.A., 2009. Permeability, relative permeability, microscopic displacement efficiency, and pore geometry of M_1 bimodal pore systems in Arab D Limestone. SPE J. 14 (3), 524–531.

Delfiner, P., 2007. Three statistical pitfalls of Phi–K transforms. SPE 102093.

Feder, J., 1988. Fractals. Plenum Press, New York.

Huet, C.C., Rushing, J.A., Newsham, K.E., Blasingame, T.A., 2005. A modified purcell/burdine model for estimating absolute permeability from mercury injection capillary pressure data, IPTC 10994. Proceedings IPTC, November Doha, Qatar.

Korvin, G., 1992. Fractal Models in the Earth Sciences. Elsevier, Amsterdam.

Mandelbrot, B.B., 1975. How long is the coast of Britain? Statistical self-similarity and fractional dimension. Science 156, 636–638.

Purcell, W.R., 1949. Capillary pressures—their measurement using mercury and the calculation of permeability therefrom. Trans. AIME 186, 39–48.

Swanson, B.F., 1981.A simple correlation between permeabilities and mercury capillary pressures, JPT, December, 2488–2504.

Thomeer, J.H.M., 1960. Introduction of a pore geometrical factor defined by the capillary pressure curve. Trans. AIME 213, 354–358.

Thomeer, J.H.M., 1983. Air permeability as a function of three pore-network parameters. JPT, April, 809–814.

Turcotte, D.L., 1992. Fractals and Chaos in Geology and Geophysics. Cambridge University Press.

Wu, Y.S., van Vliet, L.J., Frijlink, H.W., van der Voort Maarschalk, K., 2006. The determination of relative path length as a measure for tortuosity in compacts using image analysis. Eur. Pharm. Sci. 28, 433–440.

Wyllie, M.R.J., Gardner, G.H.F., 1958. The generalized Kozeny–Carman equation, its application to problems of multi-phase flow in porous media. World Oil 146 (121–128), 210–228.

[1] In case $Q_d < 0$ this would not be possible.